Journal of Applied Mechanics and Technical Physics, Vol. 48, No. 5, pp. 743–750, 2007

NUMERICAL MODELING OF THE THERMOMECHANICAL BEHAVIOR OF STEELS WITH ALLOWANCE FOR THE PROPAGATION OF LUDERS BANDS

R. R. Balokhonov[1,2] **and V. A. Romanova**[1,2]

UDC 531.3

A thermomechanical model based on physical representations of the motion of dislocation continuum and a model for the initiation and propagation of plastic shear are proposed to describe slow flows of the type of Luders bands. Two-dimensional calculations of Luders band propagation are performed for HSLA-65 steel samples under compression at various strain rates and temperatures. The calculation results are in good agreement with experimental data.

Key words: *numerical modeling, Luders bands, relaxation constitutive equation, rate and temperature sensitivity.*

Introduction. Constructing physicomechanical models of homogeneous deformation that describe the mechanical behavior of metals and alloys at various rates and temperatures is an important problem of modern mechanics. From a physical point of view, it is also necessary to develop approaches to modeling inhomogeneous flows. Substantially inhomogeneous deformation is exemplified by the propagation of Chernov–Luders localized plastic deformation bands. In experiments, a Luders band is usually observed as a macroscopic zone of localized plastic deformation, which forms near the base macroscopic stress concentrator (as a rule, near the tensile grip) and propagates throughout the sample at a rate characteristic of the particular grade of steel.

The goal of the work is to construct a combined model for the mechanical behavior of metals that includes a relaxation equation taking into account the rate and temperature sensitivity and describes the initiation and propagation of localized plastic deformation bands.

General System of Equations and Initial and Boundary Conditions. To describe material deformation, we use the system of equations including the laws of conservation of mass and momentum, strain relations, and the constitutive equations describing the material. The mechanical behavior of the examined steel grade is modeled for a plane strain state. A numerical solution is constructed in Lagrangian variables using a finite difference method [1, 2].

In the case of plane strain, the following strain rate tensor components are nonzero:

$$\dot{\varepsilon}_{11} = \dot{u}_{1,1}, \qquad \dot{\varepsilon}_{22} = \dot{u}_{2,2}, \qquad \dot{\varepsilon}_{12} = (\dot{u}_{1,2} + \dot{u}_{2,1})/2$$

(u_1 and u_2 are the displacement vector components; the dot denotes the derivative with respect to time, and the comma in the subscript denotes the derivative with respect to the coordinate).

The laws of conservation of momentum are written as

$$\sigma_{11,1} + \sigma_{21,2} = \rho\ddot{u}_1, \qquad \sigma_{12,1} + \sigma_{22,2} = \rho\ddot{u}_2.$$

The continuity equation implies

$$\dot{V}/V = \dot{\varepsilon}_{11} + \dot{\varepsilon}_{22}.$$

Here σ_{ij} are the stress tensor components, V is the specific volume, and ρ is the density.

[1]Institute of Strength Physics and Materials Science, Siberian Division, Russian Academy of Sciences, Tomsk 634021. [2]Tomsk State University, Tomsk 634050; rusy@ispms.tsc.ru; varvara@ispms.tsc.ru. Translated from Prikladnaya Mekhanika i Tekhnicheskaya Fizika, Vol. 48, No. 5, pp. 146–155, September–October, 2007. Original article submitted December 16, 2005; revision submitted September 10, 2006.

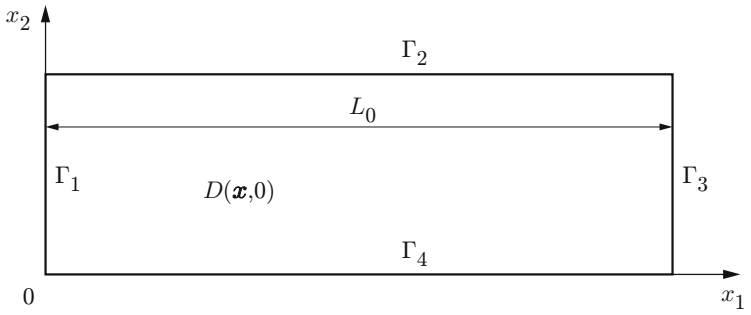

Fig. 1. Computation region (4×1 cm) and initial and boundary conditions.

Taking into account the decomposition of the stress tensor into the spherical and deviator components: $\sigma_{ij} = -P\delta_{ij} + S_{ij}$, the decomposition of the total strain rates tensor into the elastic and plastic components: $\dot{\varepsilon}_{ij} = \dot{\varepsilon}^e_{ij} + \dot{\varepsilon}^p_{ij}$, and the plastic incompressibility hypotheses ($\dot{\varepsilon}^p_{kk} = 0$), we write the pressure and stress tensor deviator components as

$$\dot{P} = -K\dot{\varepsilon}_{kk},$$

$$\dot{S}_{11} = 2\mu\Big(\dot{\varepsilon}_{11} - \frac{1}{3}\frac{\dot{V}}{V} - \dot{\varepsilon}^p_{11}\Big), \qquad \dot{S}_{22} = 2\mu\Big(\dot{\varepsilon}_{22} - \frac{1}{3}\frac{\dot{V}}{V} - \dot{\varepsilon}^p_{22}\Big), \tag{1}$$

$$\dot{S}_{12} = 2\mu(\dot{\varepsilon}_{12} - \dot{\varepsilon}^p_{12}), \qquad \dot{S}_{33} = -(\dot{S}_{11} + \dot{S}_{22}).$$

Here K and μ are the bulk compression and shear moduli and δ_{ij} is the Kronecker symbol; the summation is performed over repeated indices.

Let us consider the region $D(\boldsymbol{x}, t)$ with the boundary $\Gamma(\boldsymbol{x}, t) = \Gamma_1 \cup \Gamma_2 \cup \Gamma_3 \cup \Gamma_4$, where $\boldsymbol{x}$ is the radius-vector and t is time (Fig. 1). For $t = 0$, the initial conditions for any $\boldsymbol{x} \in D(\boldsymbol{x}, 0)$ are given by

$$\dot{u}_i(\boldsymbol{x}) = 0, \qquad \sigma_{ij}(\boldsymbol{x}) = 0, \qquad \rho(\boldsymbol{x}) = \rho^0(\boldsymbol{x}) \qquad (i, j = 1, 2),$$

where ρ^0 is the initial density.

The rates on the part of the surface $\Gamma_1 \cup \Gamma_3 \cup \Gamma_4$ and the stress on Γ_2 (Fig. 1) were specified as the boundary conditions. Uniaxial compression of the sample in the x direction is modeled on the left and right surfaces, and symmetry and free-surface conditions are modeled on the lower and upper surfaces, respectively:

$$\text{for } t \geqslant 0,\ \boldsymbol{x} \in \Gamma_1, \quad \dot{u}_1(\boldsymbol{x}, t) = \text{const} = -v;$$
$$\text{for } t \geqslant 0,\ \boldsymbol{x} \in \Gamma_3, \quad \dot{u}_1(\boldsymbol{x}, t) = \text{const} = v;$$
$$\text{for } t \geqslant 0,\ \boldsymbol{x} \in \Gamma_2, \quad \sigma_{ij}(\boldsymbol{x}, t) \cdot \boldsymbol{n}_j = 0;$$
$$\text{for } t \geqslant 0,\ \boldsymbol{x} \in \Gamma_4, \quad \dot{u}_2(\boldsymbol{x}, t) = 0;$$
$$\text{for } t \geqslant 0,\ \boldsymbol{x} \in \Gamma_1 \cup \Gamma_3 \cup \Gamma_4, \quad \sigma_{12}(\boldsymbol{x}, t) = 0.$$

Here v is the displacement rate ($v > 0$ for external extension and $v < 0$ for external compression) and $\boldsymbol{n}_j$ is the normal to the surface Γ_2.

Relaxation Constitutive Equation. Using the flow law $\dot{\varepsilon}^p_{ij} = \dot{\lambda} S_{ij}$, which is related to the plasticity condition $f(\sigma_\text{i}, \sigma_0) = 0$, where f is the yield surface, σ_0 is the elastic limit, λ is the scalar multiplier identically equal to zero in the elastic region, we express the plastic shear rate tensor components in the following form [3]

$$\dot{\varepsilon}^p_{ij} = \frac{3}{2}\frac{\dot{\varepsilon}^p_\text{i}}{\sigma_\text{i}} S_{ij}. \tag{2}$$

Here σ_i and $\dot{\varepsilon}^p_\text{i}$ are the stress intensities and plastic strain rates:

$$\sigma_\text{i} = (1/\sqrt{2})\sqrt{(\sigma_{11} - \sigma_{22})^2 + (\sigma_{22} - \sigma_{33})^2 + (\sigma_{33} - \sigma_{11})^2 + 6(\sigma^2_{12} + \sigma^2_{23} + \sigma^2_{13})},$$

$$\dot{\varepsilon}^p_\text{i} = (\sqrt{2}/3)\sqrt{(\dot{\varepsilon}^p_{11} - \dot{\varepsilon}^p_{22})^2 + (\dot{\varepsilon}^p_{22} - \dot{\varepsilon}^p_{33})^2 + (\dot{\varepsilon}^p_{33} - \dot{\varepsilon}^p_{11})^2 + 6(\dot{\varepsilon}^{p2}_{12} + \dot{\varepsilon}^{p2}_{23} + \dot{\varepsilon}^{p2}_{13})}.$$

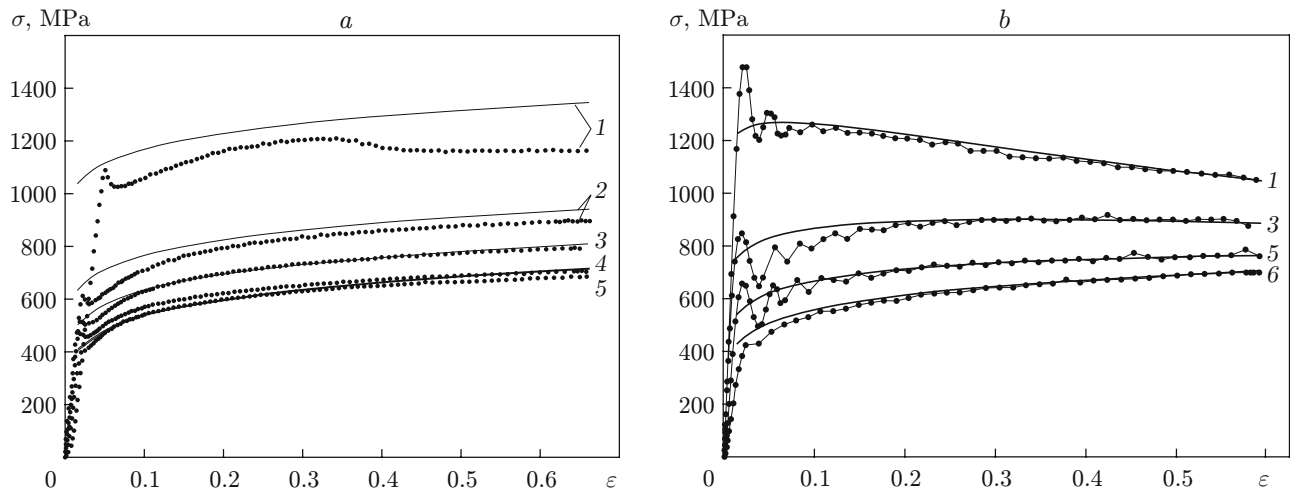

Fig. 2. Experimental stress–strain relations (points) and those calculated using model (4) (curves) for HSLA-65 steel [7] at $\dot{\varepsilon} = 0.1$ (a) and 3000 $\sec^{-1}$ (b); $T_0 = 77$ (1), 213 (2), 296 (3), 400 (4), 500 (5), and 700 K (6).

In view of (2), the constitutive relations (1) become

$$\dot{S}_{ij} = 2\mu\Big(\dot{\varepsilon}_{ij} - \frac{1}{3}\,\frac{\dot{V}}{V}\,\delta_{ij} - \frac{3}{2}\,\frac{\dot{\varepsilon}_{\mathrm{i}}^{p}}{\sigma_{\mathrm{i}}}\,S_{ij}\Big). \tag{3}$$

To close the system of equations, it is necessary to define the quantity $\dot{\varepsilon}_{\mathrm{i}}^{p}$ as a function of $\varepsilon_{\mathrm{i}}^{p}$ and σ_{i}.

Thermomechanical Model. To describe the response of the material over a wide range of temperatures ($T_0 = 77$–600) and strain rates ($\dot{\varepsilon} = 0.1$–8000 $\sec^{-1}$), we use the assumption of a dislocation nature of the plastic flow. The kinetic relations based on dislocation motion are widely used to describe the plastic strain rate [4–10]. Some theoretical assumptions on the examined problem are given in [7]. The essence of the model proposed by Nemat-Nasser and Guo [7] for the mechanical behavior of HSLA-65 steel under uniaxial compression to strain $\varepsilon > 0.6$ consists of constructing an approximating stress–strain curve with the temperature and rate sensitivity of the material taken into account.

Following [7], we denote the plastic strain rate and the stress in the one-dimensional case by $\dot{\gamma}^p$ and $\tau(\gamma^p)$, respectively. The quantity $\dot{\gamma}^p$ in [7] is used as a parameter whose variation allows to construct flow curves for various loading rates. The current stress τ is decomposed into the thermally activated component τ_T, which is due to long-range effects and does not depend on temperature, and the component τ_a due to the presence of short-range barriers preventing dislocation motion. The quantity τ_a does not depend on $\dot{\gamma}^p$ and can depend on dislocation density, grain size, the formation of substructures, etc. For the specified steel grade, Nemat-Nasser and Guo [7] employed the power law $\tau_a(\gamma^p)$. Using the expression for the energy ΔG required to overcome the barriers by means of thermal activation:

$$\Delta G = G_0[1 - (\tau_T/\tilde{\tau})^d]^q$$

and the relation [7]

$$\dot{\gamma}^p = \dot{\gamma}_r \exp\left(-\Delta G/(kT)\right),$$

we obtain

$$\tau = \tau_a + \tau_T = \tau_1(\gamma^p)^n + \tilde{\tau}\Big[1 - \Big(-\frac{kT}{G_0}\ln\frac{\dot{\gamma}^p}{\dot{\gamma}_r}\Big)^{1/q}\Big]^{1/d}, \tag{4}$$

where $\tau_1 = 760$ MPa, $n = 0.15$, $\tilde{\tau} = 1450$ MPa is the stress at which dislocations overcome the barrier without thermal activation, $G_0 = 0.8$ eV $\approx 1.28 \cdot 10^{-19}$ J is the energy sufficient to overcome the barrier only due to thermal activation, T is the temperature, $q = 2$ and $d = 2/3$ for many metals [7], k is Boltzmann's constant, and $\dot{\gamma}_r$ is a constant proportional to the density of mobile dislocations.

The flow curves $\tau(\gamma^p, \dot{\gamma}^p, T)$ calculated in [7] over a wide range of strain rates and temperature are in good agreement with experimental data for strains $\varepsilon = 0.1$–0.6 (Fig. 2). However, for $\varepsilon < 0.1$ the calculation error

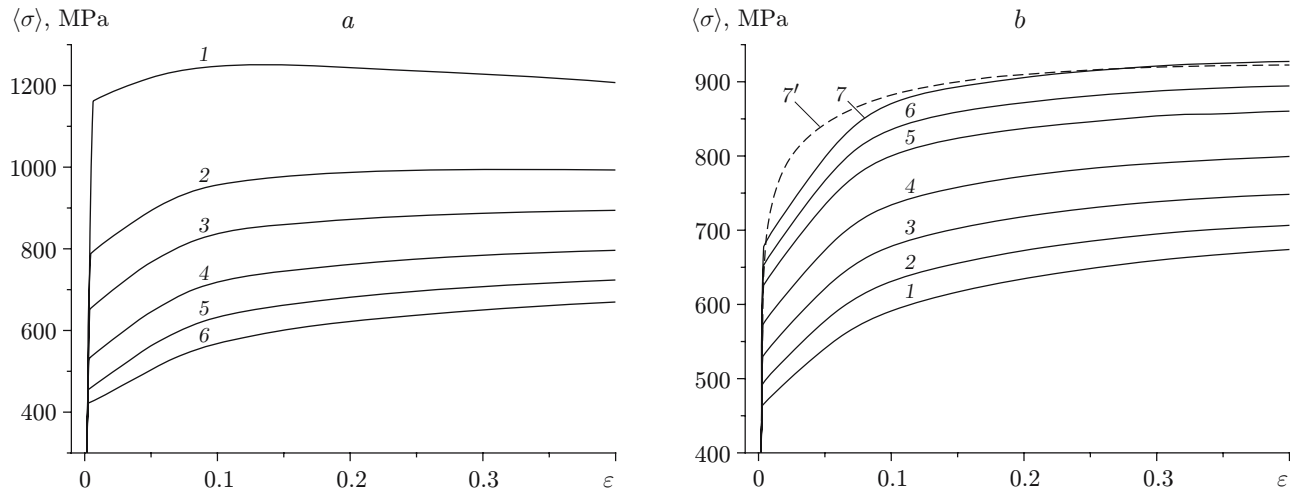

Fig. 3. Volume averaged stresses versus strains for HSLA-65 steel [calculations using model (5) ignoring Luders band propagation]: (a) for $\dot\varepsilon = 3000$ sec^{-1}, $T_0 = 77$ (1), 213 (2), 296 (3), 400 (4), 500 (5), and 600 K (6); (b) for $T_0 = 296$ K, 0.1 (1), = 1 (2), 10 (3), 100 (4), 1000 (5), 3000 (6), and 8000 (7); curve 7′ refers to the value $\dot\varepsilon = 8000$ sec^{-1} calculated using the model of [7] without introducing the fraction of mobile dislocations.

increases considerably, i.e., formula (4) leads to overestimated stresses and incorrectly describes the flow curve (Fig. 2). This can be due to the fact that the quantity $\dot\gamma_r = 4 \cdot 10^8$ sec^{-1}, which is proportional to the density of mobile dislocations N^m, is a constant in the model of [7], although N^m is known to vary in the initial stages of deformation. In addition, the experimental flow curve are characterized by the presence of the upper and lower yield limits (Fig. 2) and an yield plateau. In the case of steels, this indicates, as a rule, the initiation and propagation of Chernov–Luders localized plastic deformation bands in the initial flow stages.

For the problems considered here, it is necessary, using formulas (4), to construct the inverse relation $\dot\gamma^p(\gamma^p, \tau, T) \sim \dot\varepsilon_{\rm i}^p(\varepsilon_{\rm i}^p, \sigma_{\rm i}, T)$.

To take into account the evolution of the dislocation continuum, we introduce the fraction of mobile dislocations $F(\varepsilon_{\rm i}^p) = F^* + (1 - F^*)\exp(-B\varepsilon_{\rm i}^p/(|g|b))$ [11, 12], so that the equality $\dot\gamma_r = \dot\gamma_r^* F^*$ is satisfied. Here $|g| = 0.5$ is the orientation multiplier, $b \simeq 3.3$ Å is the modulus of the Burgers vector, and $B = 2/(d_0 N^0)$ and $F^* = N^0 d_0/(N^* d_c)$ are constants which can estimated using the physical concepts of the free path length of dislocations before the moments of their attachment at impurities [13], for example, near grain boundaries. For the examined steel grade, $N^* = 10^{12}$ cm^{-2} and $N^0 = 10^9$ cm^{-2} are the limiting and initial dislocation densities, $d_0 = 15$ μm [7] is the average grain size, and $d_c = 1$ μm [12, 13] is the average diameter of the dislocation cells formed during the deformation.

Expressing $\dot\gamma^p$ from (4), replacing $\dot\gamma_r$ by $\dot\gamma_r^* F(\varepsilon_{\rm i}^p)$, and taking into account that, for multidimensional flows, $\tau = \sigma_{\rm i}$ and $\dot\gamma^p = \dot\varepsilon_{\rm i}^p$ [7], we obtain

$$\dot\varepsilon_{\rm i}^p = \dot\gamma_r^* F(\varepsilon_{\rm i}^p) \exp\Big\{ -\frac{G_0}{kT}\Big[1 - \Big(\frac{\sigma_{\rm i} - \tau_a(\varepsilon_{\rm i}^p)}{\tilde\tau}\Big)^d\Big]^q\Big\}. \tag{5}$$

Here

$$T = T_0 + \int\limits_0^{\varepsilon_{\rm i}^p} \frac{\beta}{\rho_0 C_V}\,\sigma_{\rm i}\, d\varepsilon_{\rm i}^p;$$

T_0 is the initial temperature, $\beta \simeq 1$ (see, e.g., [7]), $\rho_0 = 7.8$ g/sm^3 is the density, and $C_V = 0.5$ J/(g$\cdot K$) is the specific heat. To differentiate between elastic and plastic strains in two-dimensional modeling, instead of the power law [7] for τ_a [see (4)] we used the function $\tau_a(\varepsilon_{\rm i}^p) = 713 - 291\exp(\varepsilon_{\rm i}^p/0.218\,42)$, where $\tau_a(0) = \sigma_0$; the quantity τ_a is in megapascals.

Figure 3 gives integrated flow curves for various temperatures and strain rates obtained in two-dimensional calculations using the modified relation (5) [$\varepsilon = (L - L_0)/L_0$, where L_0 and L are the initial and flow lengths of the computation region]. The stress was calculated as the stress intensity averaged over the region $D(\boldsymbol{x}, t)$:

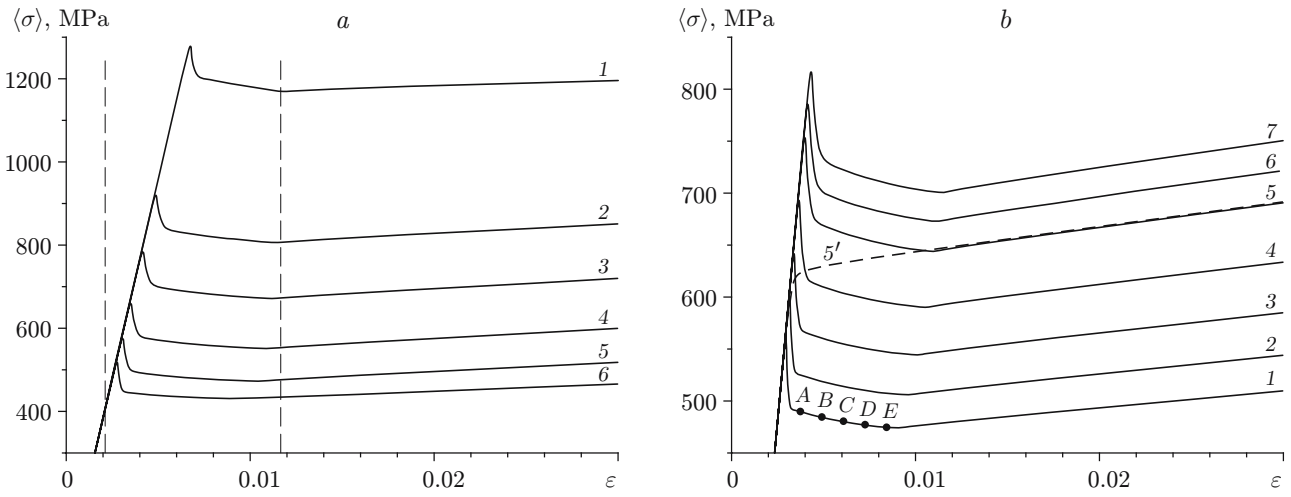

Fig. 4. Initial portions of calculated flow curves for HSLA-65 steel taking into account relation (6): (a) for $\dot{\varepsilon} = 3000$ sec^{-1}, $T_0 = 77$ (1), 213 (2), 296 (3), 400 (4), 500 (5), and 600 K (6); the region between the dashed curves is the region of initiation and propagation of a Luders band); (b) for $T_0 = 296$ K, $\dot{\varepsilon} = 0.1$ (1), 1 (2), 10 (3), 100 (4), 1000 (5); 3000 (6), and 8000 sec^{-1} (7); curve 5′ refer to the value $\dot{\varepsilon} = 1000$ sec^{-1} calculated ignoring inhomogeneous deformation.

$$\langle\sigma\rangle = \sum_{k=1,N} \sigma_{\text{i}}^k s^k \Big/ \sum_{k=1,N} s^k,$$

where N is the number of cells in the computation grid and s^k is the local volume. The strain corresponds to the relative strain of the computation region along the x_1 axis.

For comparison, the dashed curve in Fig. 3 ($T_0 = 296$ K and $\dot{\varepsilon} = 8000$ sec^{-1}) shows the dependence $\langle\sigma\rangle(\varepsilon)$ obtained in a series of test two-dimensional calculations for various strain rates and temperatures using the original model of [7] without introducing the fraction of mobile dislocations [in this case, instead of $\dot{\gamma}_r^* F(\varepsilon_{\text{i}}^p)$ in (5) the constant $\dot{\gamma}_r$ is used]. The given averaged curve and all curves for the other rates and temperatures coincide with the corresponding curves obtained in [7] using formula (4). A comparison of the calculation results of the present work (see Fig. 3) with the calculation and experimental results of [7] (see Fig. 2) leads to the conclusion that the modified relation (5) yields smaller strain resistance for $\varepsilon \leqslant 0.10$–$0.15$. Thus, this relation provides a more accurate description of experimental curves for small strains.

Luders Band Propagation. The models given above are suitable for the description of the mechanical behavior of metals and alloys in the cases where isotropic and homogeneous deformation up to failure occurs exclusively by the motion of uniformly distributed defects (dislocations) and formation of substructures. However, this formulation of continual mechanics does not allow one, without additional assumptions, to describe slow flows such as the initiation and propagation of localized plastic deformation bands.

To model the development of inhomogeneous deformation, we use an approach combining methods of continual mechanics and discrete cellular automata [14]. This approach is based on experimental data indicating that plastic strain initially arises at interfaces of an inhomogeneous material. The classical force criterion of transition from an elastic state to a plastic state in any local internal region is supplemented by the necessary condition of the presence of plastic flow, at least, in one of the adjacent regions:

$$\varepsilon_{\text{i}}^p = \varepsilon^*. \tag{6}$$

Here ε^* is the threshold plastic-strain intensity at which plastic flow can arise in a neighboring local region. The value of ε^* is to be determined experimentally by measuring local plastic strains directly behind the Luders band front or it is to be chosen during numerical modeling so that the values of the upper and lower yield limits and the extent of the yield plateau on the flow curves correspond to those observed experimentally.

In [15], condition (6) is combined with the relaxation constitutive equation without introducing the temperature explicitly. Numerical modeling of Luders band propagation in 20MnMoNi55 steel was performed for various strain rates.

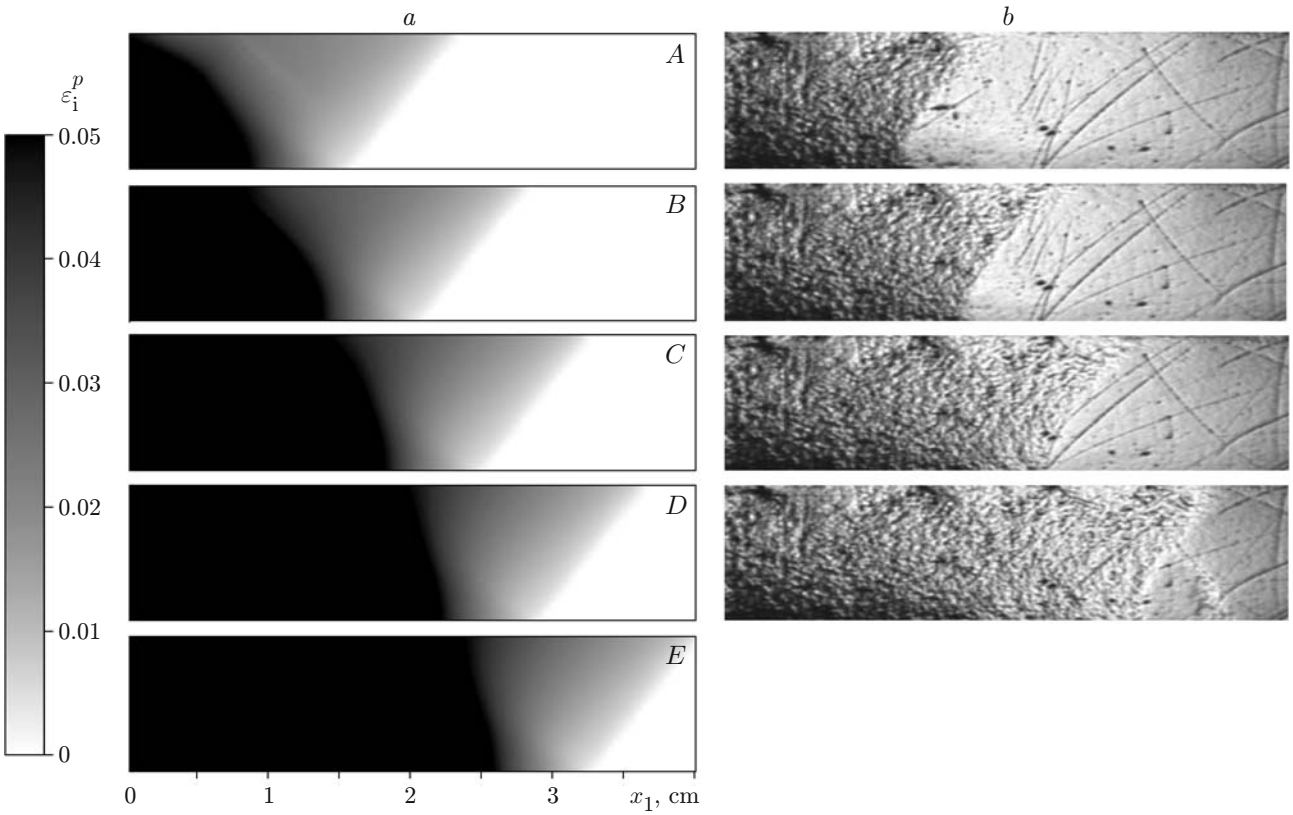

Fig. 5. Distribution of the plastic strain intensity $\varepsilon_{\mathrm{i}}^{p}$ for the propagation of the Luders band front: (a) calculation results (A–E are the material states corresponding to the points A–E in Fig. 4b); (b) the experimental data of [16].

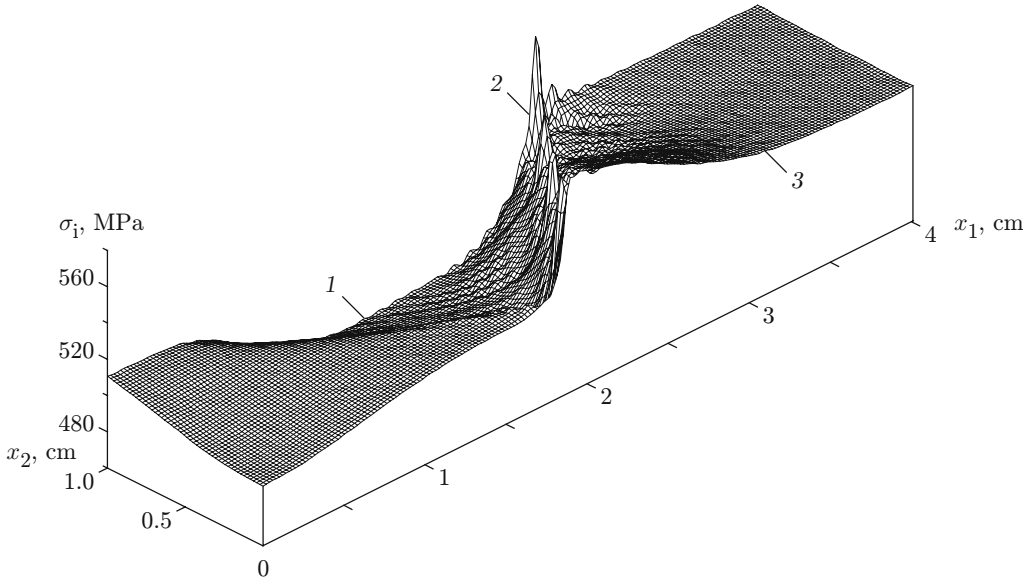

Fig. 6. Distribution of the stress intensity for the propagation of the Luders band front at the moment of compression corresponding to the point A in Fig. 4b: 1) plastic flow zone; 2) Luders band front; 3) elastic region.

In the present work, we employed a model in which criterion (6) is used together with the relaxation constitutive equation (3), which includes the plastic shear rate in the form of (5). Numerical modeling of Luders band propagation was performed over a wide range of strain rates and temperatures. Figure 4 gives the initial portions of the flow curves with allowance for Luders band propagation. The parameter $\varepsilon^* = 0.0008$. For comparison, the dashed curve in Fig. 4b ($T_0 = 296$ K and $\dot{\varepsilon} = 1000$ sec^{-1}) shows the initial portion of the curve calculated ignoring inhomogeneous deformation (see Fig. 3b). It is evident that the combined formulation provides a more accurate description of the experimental stress–strain relations for HSLA-65 steel [7] (see Fig. 2).

The plastic flow zone arises near the tensile grip (on the boundary of the computation region), and as the values of ε_{i}^p in the sample increase according to law (5), the perturbation propagates in the form of a localized plastic deformation front (Fig. 5). Plastic strain is accumulated behind the front, and elastic strain ahead of the front. Similar behavior was observed in experiments. Figure 5b shows Luders band propagation in a steel plate hardened by electron beam surfacing [16]. The plastic strain front propagates along the side face of the sample tested. In this case, the material ahead of the front is not deformed and the strain is concentrated at the moving Luders band front. This process leads to the occurrence of the upper and lower yield limits on the "macroscopic" flow curve and a zone of slow variation in the current resistance to deformation — an yield plateau (see Fig. 4).

Figure 6 shows the stress distribution at the moment corresponding to the conditions at the point A in the loading diagram (see Fig. 4). In the initial stages of Luders band propagation, the volume involved in plastic deformation is not sufficient for the total stress relaxation in the elastic region ahead of the front: here the stress intensity is higher than the current yield limit in the plastic flow region; the maximum values are observed near the front. As a result, under active loading, the stress intensity averaged over the volume continues to increase. As the plastic strain region is expanded, the stress intensity in the elastic region decreases: the Luders band front is a constant source of unloading waves, and stress relaxation occurs in the region ahead of the front. In the averaged flow curve (curve 1 in Fig. 4b), a portion appears on which the values of $\langle\sigma\rangle$ decrease. These processes of initiation and initial propagation of the localized plastic deformation front determine the formation of a yield tooth at the macrolevel (see Fig. 4).

During further loading, the stress relaxation in the elastic region (see Fig. 6) slows down. Simultaneously, the strain hardening in the expanding plastic flow region makes an increasingly greater contribution to the volume averaged stress. Therefore, an yield plateau appears in the "macroscopic" flow curve, which is characterized by a slow variation in the current resistance to deformation (see Fig. 4). In this stage, the relative elongation of the sample occur primarily by plastic deformation of the zone located behind the Luders band front.

Thus, the comparison of the experimental and calculation results shows that they are in good agreement. This indicates that the model proposed here is adequate for the examined range of strain rates and temperatures.

Conclusions. Plasticity models were considered that describe the rate and temperature sensitivities and take into account the possibility of inhomogeneous deformation during propagation of Luders bands. These phenomenological models are physically justified, take into account the collective contribution of dislocation mechanisms and describe the initiation and propagation of localized deformation bands. Calculations were performed of the elastoplastic deformation of steel samples under compression over a wide range of temperatures and strain rates: $T_0 = 77$–600 K and $\dot{\varepsilon} = 0.1$–10^4 sec^{-1}. It was shown that the introduction of the fraction of mobile dislocations and modeling Luders band propagation provides a more accurate description of the current resistance to deformation at $\varepsilon < 0.1$ and the formation of an yield tooth and plateau, in accordance with available experimental data.

This work was supported by the Russian Foundation for Basic Research (Grant No. 06-03-00592).

REFERENCES

1. M.L. Wilkins, "Calculation of elastoplastic flows," in: B. Alder, S. Fernbuch, and M. Retenberg (eds.), *Methods in Computational Physics*, Academic Press (1964).
2. R. Richtmyer and K. Morton, *Difference Methods for Initial-Value Problems*, John Wiley and Sons, New York–London–Sidney (1967).
3. O. I. Terebushko, *Fundamentals of the Theory of Elasticity and Plasticity* [in Russian], Nauka, Moscow (1984).
4. J.J. Gilman "Progress in the microdynamical theory of plasticity," in: *Proc. 5th National Congress of Applied Mechanics*, ASME, New York (1966).

5. J. M. Kelly and P. P. Gillis, "Continuum descriptions of dislocations under stress reversals," *J. Appl. Phys.*, **45**, No. 3, 1091–1096 (1974).
6. L. E. Popov, V. S. Kobytev, and T. A. Kovalevskaya, *Plastic Deformation of Alloys* [in Russian], Metallurgiya, Moscow (1984).
7. S. Nemat-Nasser and W. Guo, "Thermomechanical response of HSLA-65 steel plates: Experiment and modeling," *Mech. Mat.*, **37**, 379–405 (2005).
8. A. Molinari and G. Ravichandran, "Constitutive modeling of high-strain-rate strain in metals based on the evolution of an effective microstructural length," *Mech. Mat.*, **37**, 737–752 (2005).
9. F. H. Abed and G. Z. Voyiadjis, "Plastic strain modeling of AL-6XN stainless steel at low and high strain rates and temperatures using a combination of bcc and fcc mechanisms of metals," *Int. J. Plast.*, **21**, 1618–1639 (2005).
10. W. Guo and S. Nemat-Nasser, "Flow stress of Nitronic-50 stainless steel over a wide range of strain rates and temperatures," *Mech. Mat*, **38**, 1090–1103 (2006).
11. P. V. Makarov, "Approach of physical mezomechanics to modeling deformation and fracture processes," *Fiz. Mezomekh.*, **1**, No. 1, 61–81 (1998).
12. R. R. Balakhonov, "Modeling flow curves of metals and alloys with the packing defect energy taken into account," *Fiz. Mezomekh.*, **1**, No. 2, 73–80 (1998).
13. R. Cahn, *Physical Metallurgy*, Amsterdam (1965).
14. P. V. Makarov, V. A. Romanova, and R. R. Balokhonov, "Modeling inhomogeneous plastic deformation with the initiation of localized plastic shears at interfaces taken into account," *Fiz. Mezomekh.*, **4**, No. 5, 29–39 (2001).
15. R. R. Balokhonov, V. A. Romanova, S. Schmauder, and P. V. Makarov, "Simulation of meso-macro dynamic behavior using steel as an example," *Comput. Mat. Sci.*, **28**, 505–511 (2003).
16. S. V. Panin, V. G. Durakov, and G. A. Pribytkov, "Mesomechanics of plastic deformation and fracture of low-carbon steel with a high-strength deformable coating," *Fiz. Mezomekh.*, **1**, No. 2, 51–58 (1998).